

Efficient and stable activation by microwave annealing of nanosheet silicon doped with phosphorus above its solubility limit

Cite as: Appl. Phys. Lett. **121**, 052103 (2022); <https://doi.org/10.1063/5.0099083>

Submitted: 14 May 2022 • Accepted: 15 July 2022 • Published Online: 03 August 2022

Chun-Hsiung Tsai, Chandrashekar P. Savant, Mohammad Javad Asadi, et al.



View Online



Export Citation



CrossMark

ARTICLES YOU MAY BE INTERESTED IN

[Ultra-broadband frequency up-converter based on AlGaAs\GaAs heterojunction detector](#)


Applied Physics Letters **121**, 051106 (2022); <https://doi.org/10.1063/5.0098086>

[\$\beta\$ -Ga₂O₃ FinFETs with ultra-low hysteresis by plasma-free metal-assisted chemical etching](#)

Applied Physics Letters **121**, 052102 (2022); <https://doi.org/10.1063/5.0096490>

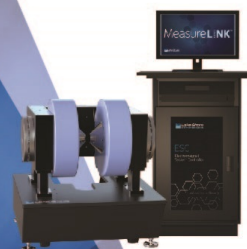
[Microscopic nonlinear magnonic phase shifters based on ultrathin films of a magnetic insulator](#)

Applied Physics Letters **121**, 052403 (2022); <https://doi.org/10.1063/5.0100525>

 **Measure Ready**
MCS-EMP Modular Characterization Systems

NEW

Multi-purpose platforms for
automated variable-field experiments





Find out more

AIP
Publishing

Efficient and stable activation by microwave annealing of nanosheet silicon doped with phosphorus above its solubility limit

Cite as: Appl. Phys. Lett. **121**, 052103 (2022); doi: [10.1063/5.0099083](https://doi.org/10.1063/5.0099083)

Submitted: 14 May 2022 · Accepted: 15 July 2022 ·

Published Online: 3 August 2022



View Online



Export Citation



CrossMark

Chun-Hsiung Tsai,¹ Chandrashekhar P. Savant,² Mohammad Javad Asadi,³ Yu-Ming Lin,⁴ Ivan Santos,⁵  Yu-Hsiang Hsu,¹  Jeffrey Kowalski,⁷ Lourdes Pelaz,⁵  Wei-Yen Woon,^{8,a)}  Chih-Kung Lee,^{1,a)}  and James C. M. Hwang^{2,3,9,a)} 

AFFILIATIONS

¹Institute of Applied Mechanics, National Taiwan University, Taipei, Taiwan

²Department of Materials Science and Engineering, Cornell University, Ithaca, New York 14853, USA

³School of Electrical and Computer Engineering, Cornell University, Ithaca, New York 14853, USA

⁴Research & Development, Taiwan Semiconductor Manufacturing Company, Hsinchu, Taiwan

⁵Department of Electronics, University of Valladolid, Valladolid, Spain

⁶Department of Electrical Engineering, National Taiwan University, Taipei, Taiwan

⁷DSC Technologies, Inc., San Jose, California 95131, USA

⁸Department of Physics, National Central University, Jungli, Taiwan

⁹International College of Semiconductor Technology, National Yang Ming Chiao Tung University, Hsinchu, Taiwan

^{a)} Authors to whom correspondence should be addressed: wywoon@phy.ncu.edu.tw; cklee@ntumems.ent; and jch263@cornell.edu

ABSTRACT

The relentless scaling of semiconductor devices pushes the doping level far above the equilibrium solubility, yet the doped material must be sufficiently stable for subsequent device fabrication and operation. For example, in epitaxial silicon doped above the solubility of phosphorus, most phosphorus dopants are compensated by vacancies, and some of the phosphorus-vacancy clusters can become mobile around 700 °C to further cluster with isolated phosphorus ions. For efficient and stable doping, we use microwave annealing to selectively activate metastable phosphorus-vacancy clusters by interacting with their dipole moments, while keeping lattice heating below 700 °C. In a 30-nm-thick Si nanosheet doped with $3 \times 10^{21} \text{ cm}^{-3}$ phosphorus, a microwave power of 12 kW at 2.45 GHz for 6 min resulted in a free-electron concentration of $4 \times 10^{20} \text{ cm}^{-3}$ and a junction more abrupt than 4 decades/nm. The doping profile is stable with less than 4% variation upon thermal annealing around 700 °C for 5 min. Thus, microwave annealing can result in not only efficient activation and abrupt profile in epitaxial silicon but also thermal stability. In comparison, conventional rapid thermal annealing can generate a junction as abrupt as microwave annealing but 25% higher sheet resistance and six times higher instability at 700 °C.

Published under an exclusive license by AIP Publishing. <https://doi.org/10.1063/5.0099083>

In shrinking the size of semiconductor devices, their free-electron concentration must also be raised higher through heavy doping of the semiconductor material with impurities as well as controlled annealing to activate the impurities into efficient donors or acceptors of charge carriers.¹ Traditionally, doping is achieved through ion implantation and activation is achieved through thermal annealing.² For scaling beyond the 3-nm node, the introduction of 3D nanostructure transistors, such as nanowire and nanosheet MOSFETs^{3,4} [Fig. 1(a)], presents

new challenges for doping and activation.^{5–10} For example, the source and drain of the MOSFETs may be doped with more than $3 \times 10^{21} \text{ P/cm}^3$, an order of magnitude higher than the equilibrium solubility of P in Si,¹¹ through *in situ* doping during epitaxial growth (see the [supplementary material](#)) instead of ion implantation.^{12–16} Although this helps to reduce the channel resistance through strain-enhanced carrier mobility, the free-electron concentration saturates due to dopant compensation while the electrical resistivity increases

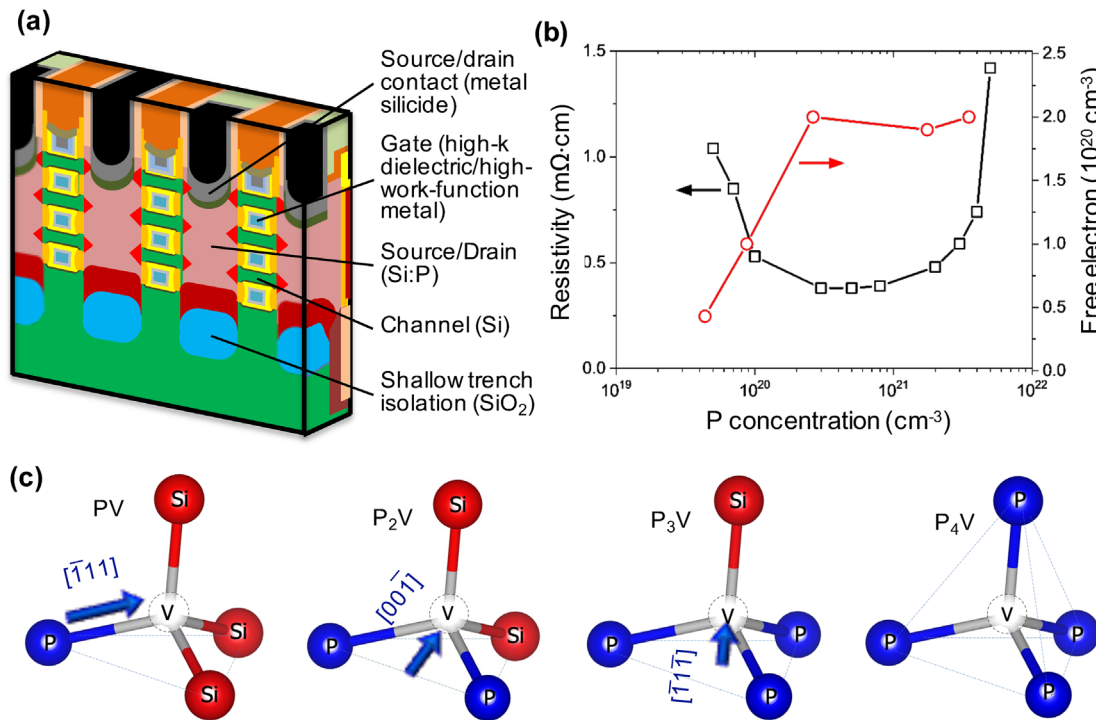
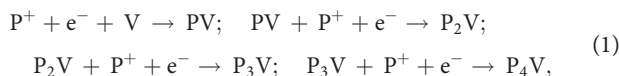


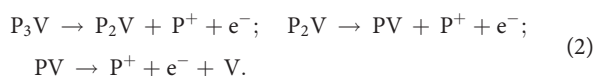
FIG. 1. Epitaxial Si:P in a 3D nanosheet transistor. (a) Cross-sectional structure of a 3D-stacked gate-all-around nanosheet transistor. (b) As-grown resistivity and free-electron concentration of Si epitaxial layers doped with different concentrations of P. (c) Tetrahedron atomic structure of P_NV clusters. Arrows indicate dipole moments except in P_4V .

due to impurity scattering [Fig. 1(b)]. Thus, with the increase in P concentration, the source and drain resistance increases rather than decreases, which renders the source and drain resistance higher than the channel resistance and the bottom nanostructure MOSFET inaccessible. Furthermore, the excess donors can become deactivated upon heating during subsequent device fabrication.^{14,17–29} The deactivation occurs because at elevated temperatures, the surface can supply vacancies to diffuse through the nanometer-thin layer to cluster with P and form P_NV complexes, thereby preventing P from being electrically active. Here, V denotes the vacancy and $N = 1, 2, 3, \text{ or } 4$. Moreover, at around 700 °C, PV, P_2V , and P_3V are sufficiently mobile²³ to continue the chain reaction to deactivate more P until they become immobile P_4V :³⁰



where e^- is the free electron. Note that P_4V is structurally similar to Si_3P_4 or Si_3N_4 .

To overcome the dopant activation/deactivation challenges, we take advantage of the dipole moments of PV, P_2V , and P_3V [Fig. 1(c)] to selectively activate them with microwave annealing^{31–36} (MWA) while keeping the temperature of the Si lattice below 700 °C to avoid forming new P_NV clusters. Thus, MWA can reverse the chain reaction of Eq. (1) to increase doping efficiency and stability:



The last step frees up the vacancy that can diffuse to the surface and be annihilated. Notice that unlike Eq. (1), Eq. (2) does not involve P_4V , which, lacking a dipole moment, cannot interact with the microwave. By contrast, conventional rapid thermal annealing (RTA, see the [supplementary material](#)) heats the lattice to near melting and recrystallization, dissociates all P_NV clusters non-selectively, and quenches in unstable PV, P_2V , and P_3V clusters upon cooling. The selectivity of MWA to dipoles is the key distinction from RTA.

Equations (1) and (2) present a simplified picture. In reality, the thermodynamics, charging states, and kinetics of all defects involved, such as P, V, PV, P_2V , P_3V , and P_4V , are complicated and not fully quantified. It has been shown by positron annihilation spectroscopy (PAS, the [supplementary material](#)) that in annealing heavily P-doped Si, P_3V clusters start to form around 527 °C and start to dissociate around 627 °C.²³ This is because the formation energy of a vacancy is reduced by its binding energy with P. Similarly, P_2V and PV clusters can be formed when annealed to higher temperatures but quenched to room temperature. Since these quenched-in PV, P_2V , and P_3V clusters all have formation and migration energies around 1 eV, upon reheating to the 500–700 °C range, they can diffuse around to gather more P until becoming stable P_4V . Thus, reheating to 700 °C constitutes a severe test for dopant deactivation and the thermal budget for postprocessing. Note that 700 °C is an order-of-magnitude estimate and the extent of diffusion and deactivation is governed by not only temperature but also time and distance.

MWA is not just another way to heat a crystal.^{37–40} Compared to RTA of the same temperature and duration, MWA of ion-implanted Si has been found to result in more dopant activation and less dopant

diffusion (Table I).^{31–35} In the case of MWA of epitaxial Si, abrupt junction profile and stable activation was found.³⁶ These advantages of MWA have been attributed to the direct interaction of microwave with the dipole moments of vacancy clusters.³⁵ These advantages are particularly remarkable when the doping concentration exceeds the solubility limit of phosphorus^{34,36} or boron.³⁵

Efficient activation and abrupt junction by MWA have been found mainly in ion-implanted Si.^{31–35} Our results not only confirm the same advantages in epitaxial Si but also show additional advantage in stable activation that can withstand reheating up to 700 °C. Epitaxy is often required for 3D nanostructures. Epitaxy also avoids implantation damage and simplifies dopant activation and diffusion kinetics. Thus, rather than removing implantation damage, the focus for annealing a heavily doped epitaxial layer is on efficient activation with minimum diffusion. The additional advantage of MWA in stability is particularly important for doping concentrations above the solubility limit, which can suffer from dopant deactivation.

To better understand the MWA mechanism, we characterize the epitaxial Si in terms of not only impurity concentration and electrical resistivity as in Refs. 31–36 but also strain by high-resolution x-ray diffraction (HRXRD, see the supplementary material), and vacancy concentration and electronic environment by PAS (the supplementary material). Additionally, we confirm the selective activation of low- N P_NV clusters through *ab initio* calculations (the supplementary material) of their formation energies and dipole moments. The calculations confirm that while PV and P_2V have significantly positive formation energies, P_4V has a negative formation energy and, hence, thermal stability. Moreover, the binding energy of P to all P_NV clusters is on the order of 1 eV, making it difficult to reverse Eq. (1) except by non-thermal means, such as MWA.

In this paper, we show that a 30-nm-thick Si epitaxial layer, doped with 3×10^{21} P/cm³ and annealed by a microwave power of 12 kW at 2.45 GHz for 6 min, has a free electron concentration of 4×10^{20} cm⁻³ and a junction more abrupt than 4 decades/nm. This is 25% more efficient than the same layer annealed by millisecond annealing (MSA, the supplementary material)^{41–44} using a flashlamp, which represents the state-of-the-art RTA. Meanwhile, the MWA sample is six times more stable than the MSA sample when subjected to RTA around 700 °C for 5 min.

Figure 2(a) shows schematically that the MWA setup (DSG AXOM) resembles a microwave oven with a cavity of approximately 600 mm on each side. In the middle of the cavity, three parallel susceptors are stacked with a spacing of approximately 5 mm. Each susceptor

is a 300-mm-diameter, 775- μ m-thick Si wafer coated with 225- μ m-thick SiC. The Si susceptor is doped with a conductivity of 10 S/m, so that it can be heated by a microwave signal of 12 kW and 2.45 GHz to 680 °C as measured by a pyrometer. In this case, the heating of the susceptor is mainly by the microwave-induced eddy current and the associated Ohmic loss.^{37–40} The susceptor spacing and the microwave frequency have been optimized so that a fifth-order standing wave forms between the top and bottom susceptors with the intensity peaking at the middle susceptor where the sample is placed. Figure 2(b) confirms that, under a 12.241-GHz signal, the simulated (the supplementary material) electric field distribution peaks between the top and bottom susceptors. Note that the microwave source is made of magnetrons, which are notoriously noisy and rich in harmonics. Although the simulation shows also a lateral resonance across the diameter of the susceptor, in reality the very-high-order resonance is fragile and can be smeared out by the noise of the magnetrons [Fig. 2(c)]. Experimentally, we found that MWA results in uniform sheet resistivity across the sample, but its efficiency is sensitive to the susceptor spacing and microwave frequency.

To produce a low-resistance, ultra-shallow junction for aggressive device scaling, MWA is at least equal to, if not better than, MSA. For comparison, the 30-nm-thick Si epitaxial layer doped with 3×10^{21} P/cm³ is split into two halves for MWA and MSA, respectively. Figure 3(a) shows that the impurity profile after MWA, as measured by secondary ion mass spectroscopy (SIMS, the supplementary material), has a junction slope of 4–5 decades/nm, which is comparable to the profiles as-grown and after MSA. Figure 3(b) plots the sheet resistance as measured by the four-probe Kelvin method (the supplementary material) against the junction depth. It can be seen that, compared to the MSA sample, the MWA sample has a comparable junction depth but a 25% lower sheet resistance. Additionally, the sheet resistance and junction depth appear to be insensitive to the MWA duration. For example, an additional 30 s of MWA decreases the sheet resistance by only 2% and increases the junction depth by only 5%.

The lower sheet resistance of the MWA sample is consistent with the lower P_NV concentration as correlated with the reduction of the tensile strain in Si:P.^{14–16} Figure 3(c) compares the effects of MWA and MSA on the HRXRD rocking curves of the Si:P layer. The most prominent peak at 0 arc sec is associated with bulk Si; the secondary peak, approximately 2000 arc sec higher, is associated with the Si:P layer. Compared to the curve of the as-grown sample, both MSA and MWA shift the Si:P peak toward the Si peak, indicating lower tensile strain and lower vacancy concentration. However, MWA is more

TABLE I. Advantages of MWA over RTA for dopant activation in silicon crystals.

Year	Dopant	Conc. (cm ⁻³)	Method	Freq. (GHz)	Power (W/cm ³)	Lattice temp. (°C)	Efficient activation	Abrupt junction	Stable activation	Reference
2001	B	1×10^{19}	Implant	2.45	9×10^{-3}	900–1,000		X		31
2009	B	1×10^{18}	Implant	2.45	5×10^{-2}	450–500	X			32
2011	As	4×10^{18}	Implant	2.45	5×10^{-2}	520–680		X		33
2013	P	8×10^{20}	Implant	2.45	4×10^{-2}	740		X		34
2013	B	5×10^{21}	Implant	5.8		530	X	X		35
2021	P	3×10^{21}	Epitaxy	5.8	7×10^{-2}	700		X	X	36
2022	P	3×10^{21}	Epitaxy	2.45	7×10^{-2}	680	X	X	X	This work

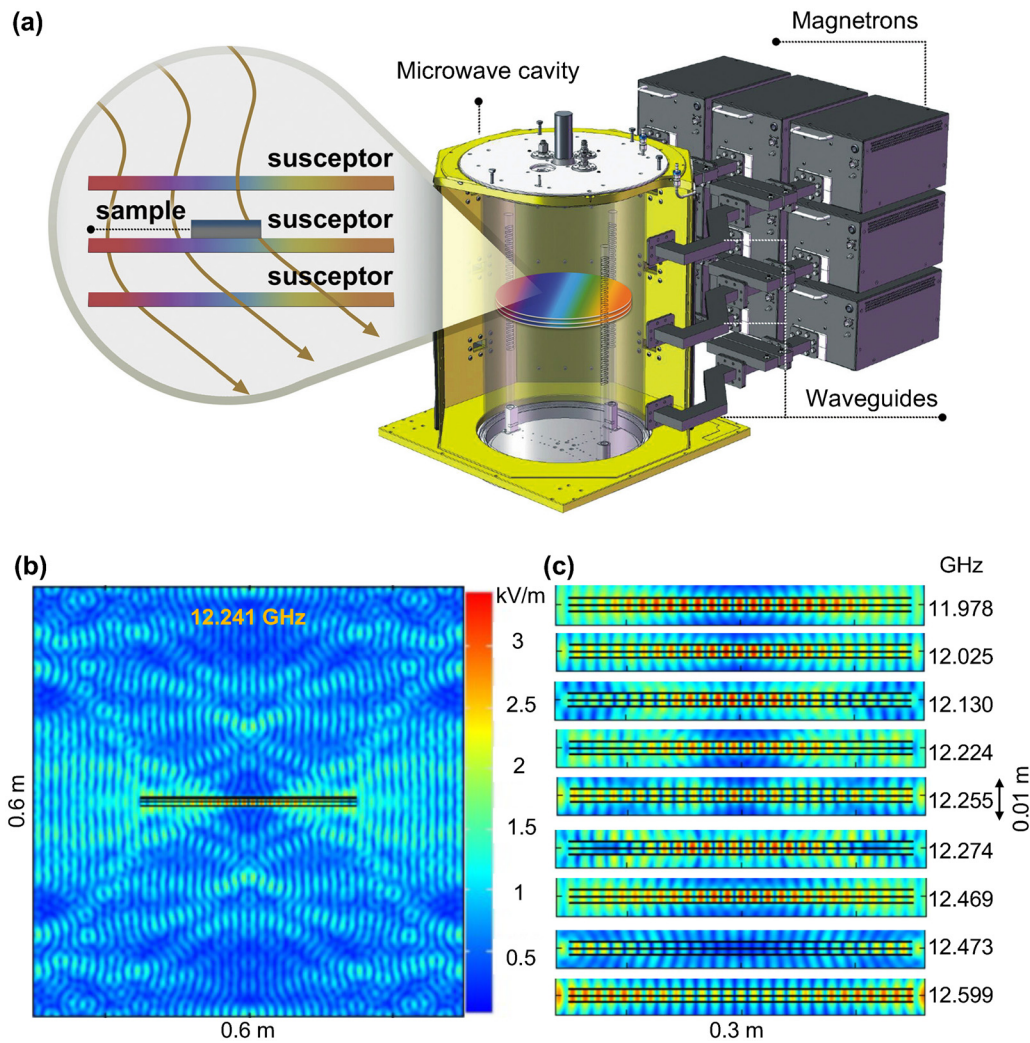


FIG. 2. Microwave annealing setup. (a) Schematics showing three closely spaced SiC-coated Si susceptors stacked in the middle of the microwave cavity and a sample placed on the middle susceptor. (b) Simulated electric field distribution over the microwave cavity showing fifth-order vertical resonance at 12.241 GHz between the top and bottom susceptors. (c) Detailed field distribution between the susceptors with the vertical dimension exaggerated and the microwave signal tuned away from 12.241 GHz, showing the lateral resonance shifts while the vertical resonance stays.

effective than MSA, and MWA of 15 kW and 150 s is more effective than MWA of 12 kW and 300 s.

MWA is more effective than MSA in dissociating PV, P₂V, and P₃V clusters as characterized by PAS.^{45,46} To circumvent calibration issues, the PAS result is summarized in the *W*-*S* plot as increasingly energetic positrons sample deeper from the surface into the bulk.^{47,48} Here, *W* and *S* are shape factors of the spectral line sensitive to core electrons and valence electrons, respectively, around the vacancy. Figure 3(d) compares the *W*-*S* plot after MWA with that as grown. In both cases, the *W*-*S* curve first follows the line of surface states and then switches over to the line of bulk states, with the turning point corresponding to where the positron is most likely trapped and annihilated. However, the *W*-*S* curve of the MWA sample turns around at a much lower *S* value, indicating a higher *N* of the P_{*N*}V cluster where

the positron is trapped and annihilated. Compared with the PAS of an MSA-annealed sample,¹⁰ this confirms that the MWA sample is dominated by high-*N* P_{*N*}V clusters, whereas the as-grown and MSA samples are dominated by low-*N* P_{*N*}V clusters.

Compared to MSA, MWA can result in not only lower resistance and higher free-electron concentration but also greater stability during device fabrication and operation. Figures 3(e) and 3(f) compare the changes in resistivity and free-electron concentration after 5 min of conventional RTA at different temperatures. Here, the resistivity is calculated by multiplying the measured sheet resistance with the layer thickness, and the free-electron concentration is characterized by Hall measurements (the supplementary material). For both MWA and MSA, the resistivity first increases up to approximately 700 °C and then decreases. However, from 550 to 750 °C, the MWA sample is

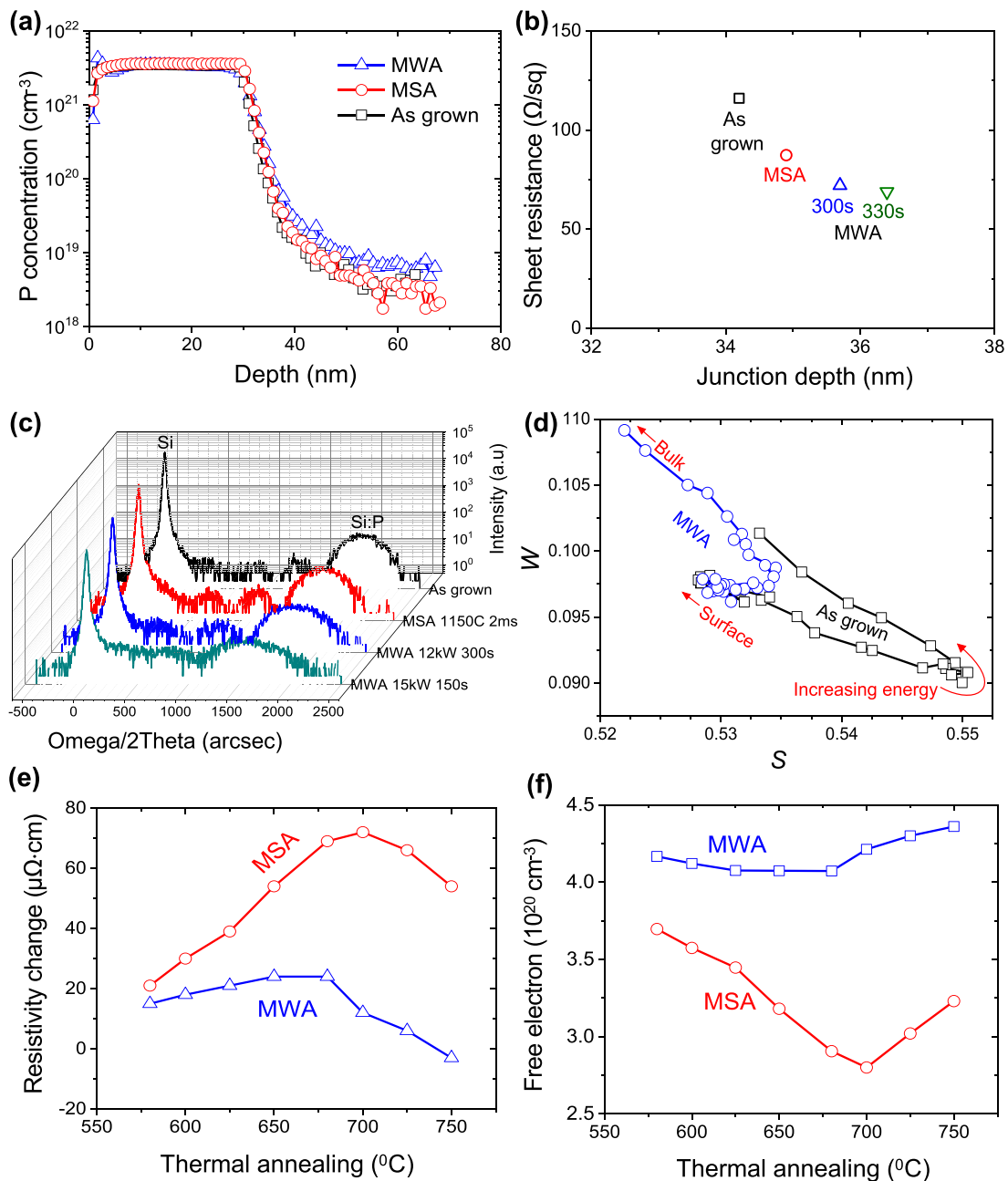


FIG. 3. Comparison of MWA and MSA of a 30-nm-thick Si epitaxial layer doped with 3×10^{21} P/cm³. (a) Depth profile of P impurity concentration showing that both MWA and MSA can result in an abrupt junction. (b) Sheet resistance vs junction depth showing MWA can result in a junction depth comparable to that of MSA but a lower sheet resistance. (c) HRXRD rocking curves showing that MWA results in greater reduction of tensile strain than MSA does. (d) PAS W - S plots showing the reduction of P_NV clusters after MWA. (e) and (f) Changes in resistivity and free-electron concentration when thermal annealed at different temperatures showing that the MWA sample is more stable than the MSA sample.

significantly more stable with a variation of approximately $18 \mu\Omega\text{-cm}$ (4%), whereas the MSA sample varies by approximately $70 \mu\Omega\text{-cm}$ (24%). Similarly, over the same temperature range, the free-electron concentration varies by 7% for the MWA sample, but by 22% for the MSA sample. The difference in temperature stability between MWA

and MSA is consistent with the hypothesis that MWA is more effective in reducing the concentration of PV, P₂V, and P₃V clusters. As mentioned before, these clusters start to form around 527 °C but can dissociate around 627 °C. This causes the resistivity to increase below 700 °C and decrease above 700 °C, while the free-electron

concentration does the opposite. However, with fewer residual PV, P₂V, and P₃V clusters in the MWA sample to begin with, it is more stable than the MSA sample against such a temperature variation.

In conclusion, we have overcome the fundamental challenge for high yet stable doping above the solubility. Our results support the hypothesis that unstable doping in thermal annealing of Si doped with P above the solubility limit is mainly due to unstable and mobile PV, P₂V, and P₃V clusters. With MWA, these clusters can be selectively eliminated while keeping the lattice temperature sufficiently low to prevent new P_NV clusters from forming. This can result in an efficient, abrupt, and stable doping in Si not only with P, but also other dopants such as B, As, Sb that can also cluster with a point defect. The same approach can also be applied to other semiconductors, such as SiGe and Ge.^{49,50} With further optimization of the MWA setup and condition, the advantages of MWA over MSA may be enlarged.

See the [supplementary material](#) for characterization and simulation methods as well as dipole moments evaluated by electronic density calculations.

The authors thank H.-J. Gossmann of Applied Materials and Paul J. Timans of Mattson Technology for insight into the thermal stability of donors discussed in this work. The authors acknowledge financial support from Ministry of Science and Technology of Taiwan under Contract No. MOST 109-2628-M-008-004-MY3.

AUTHOR DECLARATIONS

Conflict of Interest

The authors have no conflicts to disclose.

Author Contributions

Chun-Hsiung Tsai: Supervision (lead). **Chih-Kung Lee:** Investigation (equal). **James C. M. Hwang:** Writing – original draft (lead); Writing – review and editing (lead). **Chandrashekar Prakash Savant:** Investigation (equal). **Mohammad Javad Asadi:** Investigation (supporting). **Yu-Ming Lin:** Conceptualization (lead). **Iván Santos:** Investigation (equal). **Yu-Hsiang Hsu:** Investigation (equal). **Jeffrey M. Kowalski:** Investigation (equal). **Lourdes Pelaz:** Formal analysis (equal). **Wei Yen Woon:** Investigation (equal).

DATA AVAILABILITY

The data that support the findings of this study are available from the corresponding author upon reasonable request.

REFERENCES

- See <https://irds.ieee.org> for “IEEE International Roadmap for Devices and Systems” (2020).
- J. O. Borland, in *Extended Abstracts of the 3rd International Workshop Junction Technology (IWJT)* (IEEE, 2002), p. 85.
- S. D. Suk, S.-Y. Lee, S.-M. Kim, E.-J. Yoon, M.-S. Kim, M. Li, C. W. Oh, K. H. Yeo, S. H. Kim, D.-S. Shin, K.-H. Lee, H. S. Park, J. N. Han, C. J. Park, J.-B. Park, D.-W. Kim, D. Park, and B.-I. Ryu, in *IEEE International Electron Devices Meeting (IEDM)* (IEEE, 2005), p. 717.
- S.-Y. Lee, E.-J. Yoon, S.-M. Kim, C. W. Oh, M. Li, J.-D. Choi, K.-H. Yeo, M.-S. Kim, H.-J. Cho, S.-H. Kim, D.-W. Kim, D. Park, and K. Kim, in *Symposium of VLSI Technology* (IEEE, 2004), p. 200.
- W. Vandervorst, J. L. Everaert, E. Rosseel, M. Jurczak, T. Hoffman, P. Eyben, J. Mody, G. Zschätzsch, S. Koelling, M. Gilbert, T. Poon, J. del Agua Borniquel, M. Foad, R. Duffy, and B. J. Pawlak, *AIP Conf. Proc.* **1066**, 449 (2008).
- J. C. Ho, R. Yerushalmi, Z. A. Jacobson, Z. Fan, R. L. Alley, and A. Javey, *Nat. Mater.* **7**, 62 (2008).
- R. Duffy, G. Curatola, B. J. Pawlak, and G. Doornbos, *J. Vac. Sci. Technol. B* **26**, 402 (2008).
- J. C. Ho, R. Yerushalmi, G. Smith, P. Majhi, J. Bennett, J. Halim, V. N. Faifer, and A. Javey, *Nano Lett.* **9**, 725 (2009).
- J. W. Lee, Y. Sasaki, M. J. Cho, M. Togo, G. Boccardi, R. Ritzenthaler, G. Eneman, T. Chiarella, S. Brus, N. Horiguchi, G. Groeseneken, and A. Thean, *Appl. Phys. Lett.* **102**, 223508 (2013).
- L. Pelaz, L. A. Marqués, M. Aboy, P. López, and I. Santos, *Mater. Sci. Semicond. Process* **62**, 62 (2017).
- A. Mostafa and M. Medraj, *Materials* **10**, 676 (2017).
- X. Li, A. Dube, Z. Ye, S. Sharma, Y. Kim, and S. Chu, *ECS Trans.* **64**, 959 (2014).
- C.-N. Ni, X. Li, S. Sharma, K. V. Rao, M. Jin, C. Lazik, V. Banthia, B. Colombeau, N. Variam, A. Mayur, H. Chung, R. Hung, and A. Brand, in *Symposium of VLSI Technology* (IEEE, 2015), p. T118.
- S. K. Dhayalan, J. Kujala, J. Slotte, G. Pourtois, E. Simoen, E. Rosseel, A. Hikavy, Y. Shimura, S. Iacovo, A. Stesmans, R. Loo, and W. Vandervorst, *Appl. Phys. Lett.* **108**, 082106 (2016).
- E. Rosseel, S. K. Dhayalan, A. Y. Hikavy, R. Loo, H. B. Profijt, D. Kohen, S. Kubicek, T. Chiarella, H. Yu, N. Horiguchi, D. Mocuta, K. Barla, A. Thean, G. Bartlett, J. Margetis, N. Bhargava, and J. Tolle, *ECS Trans.* **75**, 347 (2016).
- M. Lee, H.-Y. Ryu, E. Ko, and D.-H. Ko, *ACS Appl. Electron. Mater.* **1**, 288 (2019).
- K. C. Pandey, A. Erbil, G. S. Cargill III, and R. F. Boehme, *Phys. Rev. Lett.* **61**, 1282 (1988).
- M. Ramamoorthy and S. T. Pantelides, *Phys. Rev. Lett.* **76**, 4753 (1996).
- V. Ranki, J. Nissilä, and K. Saarinen, *Phys. Rev. Lett.* **88**, 105506 (2002).
- Y. Takamura, S. H. Jain, P. B. Griffin, and J. D. Plummer, *J. Appl. Phys.* **92**, 230 (2002).
- Y. Takamura, P. B. Griffin, and J. D. Plummer, *J. Appl. Phys.* **92**, 235 (2002).
- V. Ranki, K. Saarinen, J. Fage-Pedersen, J. Lundsgaard Hansen, and A. Nylandsted Larsen, *Phys. Rev. B* **67**, 041201(R) (2003).
- V. Ranki and K. Saarinen, *Phys. Rev. Lett.* **93**, 255502 (2004).
- D. C. Mueller and W. Fichtner, *Phys. Rev. B* **70**, 245207 (2004).
- V. Ranki, A. Pelli, and K. Saarinen, *Phys. Rev. B* **69**, 115205 (2004).
- M. Rummukainen, I. Makkonen, V. Ranki, M. J. Puska, K. Saarinen, and H.-J. L. Gossmann, *Phys. Rev. Lett.* **94**, 165501 (2005).
- B. Sahli, K. Vollenweider, and W. Fichtner, *Phys. Rev. B* **80**, 075208 (2009).
- M. T. Björk, H. Schmid, J. Knoch, H. Riel, and W. Riess, *Nat. Nanotechnol.* **4**, 103 (2009).
- R. Chen, B. Trzynadlowski, and S. T. Dunham, *J. Appl. Phys.* **115**, 054906 (2014).
- Z. Ye, S. Chopra, R. Lapena, Y. Kim, and S. Kuppuraio, *ECS Trans.* **50**, 1007 (2013).
- K. Thompson, J. H. Booske, D. F. Downey, Y. Gianchandani, and R. Cooper, in *Proceedings of 199th Meeting, Electrochemical Society: Rapid Thermal and Other Short-Time Processing Technologies II* (IEEE, 2001), p. 121.
- T. L. Alford, D. C. Thompson, J. W. Mayer, and N. D. Theodore, *J. Appl. Phys.* **106**, 114902 (2009).
- R. N. P. Vemuri, M. J. Gadre, N. D. Theodore, W. Chen, S. S. Lau, and T. L. Alford, *J. Appl. Phys.* **110**, 034907 (2011).
- Z. Zhao, N. D. Theodore, R. N. P. Vemuri, S. Das, W. Lu, S. S. Lau, and T. L. Alford, *Appl. Phys. Lett.* **103**, 192103 (2013).
- P. Xu, C. Fu, C. Hu, D. W. Zhang, D. Wu, J. Luo, C. Zhao, Z.-B. Zhang, and S.-L. Zhang, *Appl. Phys. Lett.* **102**, 122114 (2013).
- C. H. Tsai, Y. H. Hsu, I. Santos, L. Pelaz, J. E. Kowalski, J. W. Liou, W. Y. Woon, and C. K. Lee, *Mater. Sci. Semicond. Process.* **127**, 105672 (2021).
- U. Chandra, *Microwave Heating* (InTech, 2011).
- R. R. Mishra and A. K. Sharma, *Composites, Part A* **81**, 78 (2016).
- C. Fu, Y. Wang, P. Xu, L. Yue, F. Sun, D. W. Zhang, S.-L. Zhang, J. Luo, C. Zhao, and D. Wu, *AIP Adv.* **7**, 035214 (2017).

- ⁴⁰A. Nozariasbmarz, K. Dsouza, and D. Vashaee, *Appl. Phys. Lett.* **112**, 093103 (2018).
- ⁴¹W. Lerch, S. Paul, J. Niess, S. McCoy, T. Selinger, J. Gelpey, F. Cristiano, F. Severac, M. Gavelle, S. Boninelli, P. Pichler, and D. Bolze, *Mater. Sci. Eng. B* **124–125**, 24 (2005).
- ⁴²T. Miyashita, T. Kubo, Y. S. Kim, M. Nishikawa, Y. Tamura, J. Mitani, M. Okuno, T. Tanaka, H. Suzuki, T. Sakata, T. Kodama, T. Itakura, N. Idani, T. Mori, Y. Sambonsugi, A. Shimizu, H. Kurata, and T. Futatsugi, in *IEEE International Electron Devices Meeting (IEDM) Technical Digest* (IEEE, 2009), p. 27.
- ⁴³S. Govindaraju, C.-L. Shih, P. Ramanarayanan, Y.-H. Lin, and K. Knutson, *ECS Trans.* **28**, 81 (2010).
- ⁴⁴S. Stathopoulos, L. Tsetseris, N. Pradhan, B. Colombeau, and D. Tsoukalas, *J. Appl. Phys.* **118**, 135710 (2015).
- ⁴⁵K. Saarinen, P. Hautajarvi, and C. Corbel, *Semicond. Semimetals* **51A**, 209 (1998).
- ⁴⁶F. Tuomisto and I. Makkonen, *Rev. Mod. Phys.* **85**, 1583 (2013).
- ⁴⁷S. Eichler, J. Gebauer, F. Börner, A. Polity, R. Krause-Rehberg, E. Wendler, B. Weber, W. Wesch, and H. Börner, *Phys. Rev. B* **56**, 1393 (1997).
- ⁴⁸T. Kalliovaara, J. Slotte, I. Makkonen, J. Kujala, F. Tuomisto, R. Milazzo, G. Impellizzeri, G. Fortunato, and E. Napolitani, *Appl. Phys. Lett.* **109**, 182107 (2016).
- ⁴⁹S.-L. Sihto, J. Slotte, J. Lento, K. Saarinen, E. V. Monakhov, A. Y. Kuznetsov, and B. G. Svensson, *Phys. Rev. B* **68**, 115307 (2003).
- ⁵⁰A. Vohra, A. Khanam, J. Slotte, I. Makkonen, G. Pourtois, R. Loo, and W. Vandervorst, *J. Appl. Phys.* **125**, 025701 (2019).